NANO LETTERS

pubs.acs.org/NanoLett Letter

Microscopic Theory of Multimode Polariton Dispersion in Multilayered Materials

Arkajit Mandal,* Ding Xu, Ankit Mahajan, Joonho Lee, Milan Delor, and David R. Reichman*

Cite This: *Nano Lett.* 2023, 23, 4082−4089 Read Online

ACCESS | Metrics & More | Article Recommendations | Supporting Information

ABSTRACT: We develop a microscopic theory for the multimode polariton dispersion in materials coupled to cavity radiation modes. Starting from a microscopic light−matter Hamiltonian, we devise a general strategy for obtaining simple matrix models of polariton dispersion curves based on the structure and spatial location of multilayered 2D materials inside the optical cavity. Our theory exposes the connections between seemingly distinct models that have been employed in the literature and resolves an ambiguity that has arisen concerning the experimental description of the polaritonic band structure. We demonstrate the applicability of our theoretical formalism by fabricating various geometries of multilayered perovskite materials coupled to cavities and demonstrating that our theoretical predictions agree with the experimental results presented here.

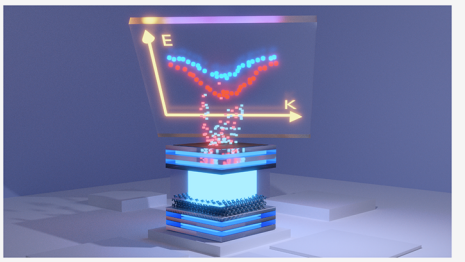

KEYWORDS: *polariton, dispersion, light−matter interactions, exciton-polaritons*

Strongly coupling matter to quantized radiation via an optical cavity leads to the formation of polaritons and enables the generation of exciting new chemical[1−11] and physical phenomena[12−20] in a highly controllable manner. Despite decades of research on polaritons, many aspects of polariton physics remain elusive.[10,21,22]

The polariton dispersion in a Fabry−Pérot cavity for a single mode coupled to a one-dimensional excitonic chain model with orientation parallel to the cavity mirrors is obtained by diagonalizing a simple 2×2 matrix.[21−25] The diagonal elements of this 2×2 matrix (one for the photon and another for the exciton) correspond to the uncoupled excitonic and photonic energies at a particular longitudinal wavevector, and the off-diagonal terms capture the light−matter coupling. When considering N cavity modes coupled to an exciton chain, one may extend the 2×2 matrix to an $(N + 1) \times (N + 1)$ matrix where the single exciton couples to all N cavity modes. However, the experimentally obtained polariton dispersion often deviates from the predictions of the $(N + 1) \times (N + 1)$ model and instead is better described by a $2N \times 2N$ model.[13,21,22,26] This $2N \times 2N$ model matrix is constructed by making N copies of the exciton branch where each exciton branch couples to one cavity mode branch, such that the overall matrix is block diagonal with N 2×2 subblocks. Previously, classical Maxwell theory has been used to investigate the polariton dispersion, where the $2N \times 2N$ model appears to predict the observed polariton dispersion correctly.[22,26] However, these studies do not provide a full microscopic understanding of these effects or the origin of the $2N \times 2N$ model from the microscopic light-matter Hamiltonian or discuss its validity in relation to the spatial geometry of the material.

In this work, we develop a quantum mechanical microscopic theory to understand and predict the multimode polariton dispersion of multilayered materials coupled to radiation in a Fabry-Pérot cavity. In the following, we develop a general $(N + N_e) \times (N + N_e)$ model (with $N_e \leq N$ exciton branches) that, for specific geometries and spatial locations of multilayered materials, reduces to $(N + 2) \times (N + 2)$, $2N \times 2N$, or $(N + 1) \times (N + 1)$ models. We then show that the $(N + 1) \times (N + 1)$ model, which is derived for a single-layer material, cannot be directly used for multilayered materials often studied in experiments. We demonstrate that regardless of interlayer coupling, for filled cavities, the $2N \times 2N$ model is appropriate. Finally, we show the applicability of this theoretical formalism by preparing multilayered perovskite materials coupled to cavities with various spatial geometries inside the cavity. We show that the multimode polariton dispersion predicted by our theoretical model agrees reasonably well with the experimental results provided here.

Here we consider a generalized Tavis−Cummings[10,16,27] (GTC) Hamiltonian describing a (Frenkel) exciton−polariton system beyond the usual long-wavelength approximation,[10,16,27−29] which we rigorously derive from the p.A Hamiltonian using orbital and nuclear-centered gauge transformations, with details being provided in the Supporting

Received: March 17, 2023
Revised: April 24, 2023
Published: April 27, 2023

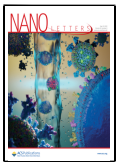

https://doi.org/10.1021/acs.nanolett.3c01017
Nano Lett. 2023, 23, 4082−4089

Information (SI). The exciton−polariton Hamiltonian of a multilayered material in a cavity with cavity quantization along y is given as

$$\hat{H}_{\mathrm{GTC}}(k_z = 0) = \sum_{k_x} \left(\sum_{k_y} \hat{a}_{\boldsymbol{k}}^{\dagger} \hat{a}_{\boldsymbol{k}} \omega_c(\boldsymbol{k}) + \sum_{m} \epsilon(k_x) \hat{d}_{k_x,m}^{\dagger} \hat{d}_{k_x,m} + \sum_{k_y,m} g_{\boldsymbol{k}} (\hat{a}_{\boldsymbol{k}}^{\dagger} \hat{d}_{k_x,m} + \hat{a}_{\boldsymbol{k}} \hat{d}_{k_x,m}^{\dagger}) \sin(k_y Y_m) \right) \equiv \sum_{k_x} \hat{h}_{\mathrm{GTC}}(k_x) \tag{1}$$

where $g_{\boldsymbol{k}} = \sqrt{N_x N_z}\, \mu_0 \lambda_{\boldsymbol{k}}$ and $\epsilon(k_x) = \omega_0 - 2\tau_z - 2\tau_x \cos(k_x\, \delta l_x)$ for a simple nearest neighbor coupling τ_x and τ_z along x and z, $\hat{d}_{k_x,m}^{\dagger}$ creates a material excitation in the mth layer located at Y_m with in-plane (with respect to the mirrors) wavevector k_x, and $\hat{a}_{\boldsymbol{k}}^{\dagger}$ is the photonic creation operator of the cavity mode $\boldsymbol{k} = (k_x, k_y, k_z)$ with photon frequency $\omega_{\boldsymbol{k}} = \frac{c}{\eta}|\boldsymbol{k}|$ (c is the speed of light and refractive index $\eta = 1$ unless otherwise noted) such that $k_x = \frac{2\pi}{L_x} n_x$ with $n_x = 0, \pm 1, \pm 2, \ldots$ with L_x as the length of the periodic supercell along x direction with a similar expression for k_z.[24] In the main text we have set $k_z = 0$ for both matter and cavity, as in most experiments (including ours) the polariton dispersion is plotted along k_x while k_z is set to 0. Further, $\boldsymbol{\lambda}_{\boldsymbol{k}} = \sqrt{\frac{\hbar \omega_c(\boldsymbol{k})}{\varepsilon_0 \varepsilon_r \mathcal{V}}}\, \hat{\boldsymbol{e}}_{\boldsymbol{k}}$, where ε_0 and ε_r are the vacuum and material permittivity, respectively, $\mathcal{V} = L_x L_y L_z$ is the quantization volume, and $\hat{\boldsymbol{e}}_{\boldsymbol{k}} \perp \boldsymbol{k}$ is the polarization direction of the radiation mode $\boldsymbol{k}$. In our model, the cavity mirror imposes a boundary condition along the y direction and thus $k_y = \frac{\pi}{L_y} n_x$ with $n_y = 0, \pm 1, \pm 2, \ldots, \pm n_{y_{\max}}$ ($n_{y_{\max}}$ is a numerical cutoff).

The GTC Hamiltonian is block-diagonal in each k_x subspace containing only $\{\hat{a}_{k_x,k_y}, \hat{a}_{k_x,k_y}^{\dagger}, \hat{d}_{k_x,m}, \hat{d}_{k_x,m}^{\dagger}\}$ with $\hat{h}_{\mathrm{GTC}}(k_x)$ as the Hamiltonian in the k_x block. Despite its convenience, an undesirable feature of the GTC Hamiltonian is that it does not converge with respect to the number of cavity modes. In the SI, we show that this is due to the absence of the dipole-self-energy term in the GTC Hamiltonian and that, perhaps counterintuitively, the GTC Hamiltonian produces accurate results only when considering a small number of energetically relevant cavity modes.

For materials with an arbitrary thickness placed inside a cavity, we develop a general strategy for obtaining the polariton dispersion based on defining new matter operators that take advantage of the structure of the light−matter coupling. Consider a total multilayer width of $l_y = \delta l_y \cdot N_y$ (with interlayer distance δl_y), where $l_y \leq L_y$. Considering N energetically relevant cavity mode branches such that we restrict $n_{\min}\frac{\pi}{L_y} \leq k_y \leq n_{\max}\frac{\pi}{L_y}$, we construct the following $N_y \times N_e$ matrix (where $N_e \leq N = n_{\max} - n_{\min} + 1$) using the cavity mode functions as

$$\Lambda_{\mathrm{NO}} = \begin{bmatrix} \sin\left(\frac{\pi n_1}{L_y} Y_1\right) & \sin\left(\frac{\pi n_2}{L_y} Y_1\right) & \ldots \\ \sin\left(\frac{\pi n_1}{L_y} Y_2\right) & \sin\left(\frac{\pi n_2}{L_y} Y_2\right) & \ldots \\ \vdots & \vdots & \ldots \\ \sin\left(\frac{\pi n_1}{L_y} Y_{N_y}\right) & \sin\left(\frac{\pi n_2}{L_y} Y_{N_y}\right) & \ldots \end{bmatrix} \tag{2}$$

where Λ_{NO} is generally a nonorthogonal matrix. Note that here $\{n_1, n_2, \ldots\}$ are chosen such that the above $N_y \times N_e$ matrix contains linearly independent columns. In most cases, $N_e = N = n_{\max} - n_{\min} + 1$, so that the cavity mode functions are linearly independent. We note that while in this work we consider idealized cavity mode functions, our formalism can be extended to include more realistic ones by solving Maxwell's equations.[23,30−34]

We numerically construct the Λ_{NO} matrix by first initializing it with a single column and then adding a column only if the rank of the matrix containing this additional column increases by 1. Note that it is important to choose $n_{\min}$ and $n_{\max}$ such that only those cavity modes that are energetically relevant for the range of energy and wavevector k_x we are interested in are included. Adding off-resonant cavity modes will introduce errors that originates from the missing dipole self-energy term in the GTC Hamiltonian (see the SI).

Next, we perform a QR decomposition of Λ_{NO} to obtain the orthonormal matrix Λ_{O} (corresponding to Q). Using Λ_{O}, we define a unitary matrix U_{O} of dimension $N_y \times N_y$ such that $[U_{\mathrm{O}}]_{m,j} = [\Lambda_{\mathrm{O}}]_{m,j}$ for $j \in \{n_{\min}, n_{\min}+1, \ldots, n_{\min}+N_e\}$ and the rest of the matrix elements are chosen such that $\sum_m [U_{\mathrm{O}}]_{m,j'} \cdot [U_{\mathrm{O}}]_{m,j} = \delta_{jj'}$. Using U_{O}, we define the new matter excitation operator as

$$\hat{d}_{k_x,k_y} = \sum_{m} [U_{\mathrm{O}}]_{m,n_y} \cdot \hat{d}_{k_x,m} \tag{3}$$

where the index $k_y = \frac{\pi}{L_y} n_y$. The consequence of this transformation is that for N energetically relevant cavity modes, there are $N_e \leq N$ matter excitation operators $\{\hat{d}_{k_x,k_y}\}$, such that $k_y \in \left\{ n_{\min}\frac{\pi}{L_y}, \ldots, (n_{\min}+N_e)\frac{\pi}{L_y} \right\} \equiv \mathcal{N}_c$, which couples to the photon operators $\{\hat{a}_{k_x,k_y}\}$. The rest of the matter excitation operators $\{\hat{d}_{k_x,k_y}\}$for which $k_y \notin \mathcal{N}_c$ are dark and can be dropped from the light−matter Hamiltonian. The Hamiltonian $\hat{h}_{\mathrm{GTC}}(k_x)$ can be written (using eq 1)

$$\hat{h}_{\mathrm{GTC}}(k_x) = \sum_{k_y \in \mathcal{K}_c} \hat{a}_{k_x,k_y}^{\dagger} \hat{a}_{k_x,k_y} \omega_c(k_x, k_y) + \varepsilon(k_x) \hat{d}_{k_x,k_y}^{\dagger} \hat{d}_{k_x,k_y} + \sum_{k_{y'} \in \mathcal{N}_c} \sum_{k_y \in \mathcal{K}_c} \Omega(k_y, k_{y'}) (\hat{a}_{k_x,k_y}^{\dagger} \hat{d}_{k_x,k_{y'}} + \hat{a}_{k_x,k_y} \hat{d}_{k_x,k_{y'}}^{\dagger}) \tag{4}$$

where

$$\Omega(k_y, k_{y'}) = g_{k_x,k_y} \sum_{m} \sin(k_y Y_m) \cdot [U_{\mathrm{O}}]_{m,n_{y'}} \tag{5}$$

https://doi.org/10.1021/acs.nanolett.3c01017
Nano Lett. 2023, 23, 4082−4089

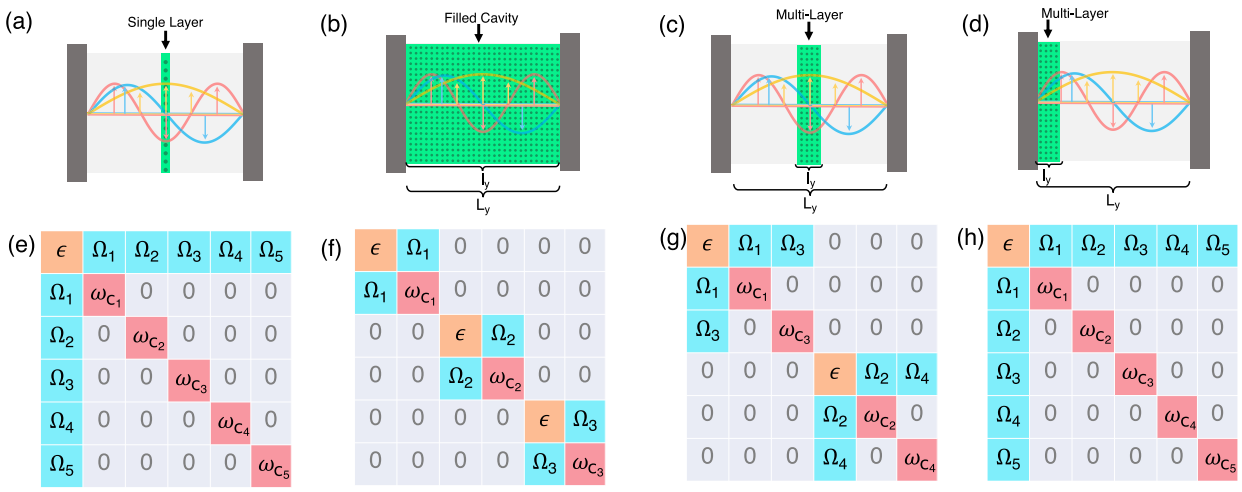

Figure 1. Schematic illustrations of various cavity setups in (a−d) and their corresponding light−matter matrixes in (e−h) that can be diagonalized to obtain multimode polariton dispersion. The solid green box represents the material of various thicknesses l_y centered at various locations: (a) a single layer material located near the center, (b) material thickness same as the length of the cavity, (c) multilayer material thickness much smaller than energetically relevant cavity mode wavelengths $l_y \ll 2\pi k_y$ located at the center of the cavity, and (d) same as (c) but located beside one of the cavity mirrors.

Here, $\mathcal{K}_c \equiv \left\{ n_{\min}\frac{9\pi}{L_y}, (n_{\min}+1)\frac{\pi}{L_y}, \ldots, n_{\max}\frac{\pi}{L_y} \right\}$ defines the subspace of energetically relevant cavity operators. Note the relation $\mathcal{N}_c \subset \mathcal{K}_c$, where $\mathcal{N}_c$ is constructed such that columns of Λ_{NO} are linearly independent (in most cases $\mathcal{N}_c \equiv \mathcal{K}_c$ and $N = N_e$).

A general $(N + N_e) \times (N + N_e)$ matrix model when using the single excited subspace spanning $\{\hat{a}^\dagger_{k_x,k_y}|G,0\rangle, \hat{d}^\dagger_{k_x,k_y}|G,0\rangle\}$ (where $|G,0\rangle$ denotes the ground state of matter with 0 cavity photons) is obtained as

$$\hat{h}_{N+N_e}(k_x) = \begin{bmatrix} \varepsilon(k_x) & \Omega\left(\frac{\pi n_1}{L_y}, \frac{\pi n_1}{L_y}\right) & 0 & \Omega\left(\frac{\pi n_1}{L_y}, \frac{\pi n_2}{L_y}\right) & \ldots \\ \Omega\left(\frac{\pi n_1}{L_y}, \frac{\pi n_1}{L_y}\right) & \omega_c\left(k_x, \frac{\pi n_1}{L_y}\right) & \Omega\left(\frac{\pi n_2}{L_y}, \frac{\pi n_1}{L_y}\right) & 0 & \ldots \\ 0 & \Omega\left(\frac{\pi n_2}{L_y}, \frac{\pi n_1}{L_y}\right) & \varepsilon(k_x) & \Omega\left(\frac{\pi n_1}{L_y}, \frac{\pi n_2}{L_y}\right) & \ldots \\ \Omega\left(\frac{\pi n_1}{L_y}, \frac{\pi n_2}{L_y}\right) & 0 & \Omega\left(\frac{\pi n_1}{L_y}, \frac{\pi n_2}{L_y}\right) & \omega_c\left(k_x, \frac{\pi n_2}{L_y}\right) & \ldots \\ \vdots & \vdots & \vdots & \vdots & \ddots \end{bmatrix} \quad (6)$$

Note that when $N_e = 1$, the above matrix reduces to the $(N + 1) \times (N + 1)$ form[26,35] (such as for a single-layer material). Meanwhile, when $N_e = N$ and for $\Omega\left(\frac{\pi m}{L_y}, \frac{\pi n}{L_y}\right) = \delta_{m,n}\Omega\left(\frac{\pi n}{L_y}, \frac{\pi n}{L_y}\right)$, the above matrix reduces to the $2N \times 2N$ (such as for a filled cavity) form.[21,22,26]

In Figure 1 we summarize the schematic forms of the Hamiltonian for various cavity setups that can be diagonalized to obtain the polariton dispersion. Using the general strategy outlined above, for a single-layer material shown in Figure 1e, we find the widely used $(N + 1) \times (N + 1)$ matrix.[21−23,26,36−39] In this model, within each k_x block, one exciton state, corresponding to $\hat{d}^\dagger_{k_x,m=0}|G,0\rangle$, is coupled to N cavity excitations $\hat{a}^\dagger_{k_x,k_y}|G,0\rangle$ via the coupling $\Omega_{n_y} = g_{\mathbf{k}} \sin\left(\frac{\pi n_y}{L_z}\cdot Y_0\right)$ where Y_0 is the position of the single layer inside cavity.

For a filled cavity, we obtain an $2N \times 2N$ matrix that includes N exciton states $\hat{d}^\dagger_{k_x,k_y}|G,0\rangle$, where $\hat{d}^\dagger_{k_x,k_y} = \frac{1}{\sqrt{\mathcal{N}_y}} \sin\left(k_y\cdot\left(m - \frac{1}{2}\right)\right)\hat{d}^\dagger_{k_x,m}$ with $\mathcal{N}_y$ as a normalization constant, that are coupled to N cavity excitations $\hat{a}^\dagger_{k_x,k_y}|G,0\rangle$. This $2N \times 2N$ matrix model contains N noninteracting 2×2 blocks as shown in Figure 1f. Therefore, in a filled cavity there exist N excitons that couple to N cavity modes of matching k_y. We also obtain the same $2N \times 2N$ model when considering interacting layers $\tau_y \neq 0$ (see detailed analytical expressions in the SI).

https://doi.org/10.1021/acs.nanolett.3c01017
Nano Lett. 2023, 23, 4082−4089

For partially filled cavities we find two interesting matrix models depending on the position of the material inside a cavity. For a thin material placed at the middle of the cavity we find a $(N+2)\times(N+2)$ matrix (Figure 1g) model which is composed of two isolated $\left(\frac{N}{2}+1\right)\times\left(\frac{N}{2}+1\right)$ blocks. One block contains one "symmetric" exciton state $\hat{d}_{k_x,S}^{\dagger}|G,0\rangle$, where $\hat{d}_{k_x,S}^{\dagger}=\frac{1}{\sqrt{N_y}}\sum_m \hat{d}_{k_x,m}^{\dagger}$ is coupled to odd cavity modes ($k_y=\frac{n_y\pi}{L_z}$ with n_y = 2, 4, 6, ...). The other block contains one "asymmetric" exciton state $\hat{d}_{k_x,A}^{\dagger}|G,0\rangle$, where $\hat{d}_{k_x,A}^{\dagger}=\frac{1}{\sqrt{\mathcal{N}}}\sum_m\left(Y_m-\frac{L_y}{2}\right)\hat{d}_{k_x,m}^{\dagger}$ that is coupled to even cavity modes. For a thin material placed next to a mirror, we obtain the $(N+1)\times(N+1)$ model which is shown in Figure 1h. In this model one exciton state $\hat{d}_{k_x,B}^{\dagger}|G,0\rangle$, where $\hat{d}_{k_x,B}=\frac{1}{\sqrt{\mathcal{N}_B}}\sum_m Y_m\hat{d}_{k_x,m}$ ($\mathcal{N}_B$ is a normalization constant), is coupled to N cavity modes. The analytical forms of the couplings are provided in the SI.

Numerical Results. Figure 2 presents numerical results for various multilayered materials. In Figure 2a–d we consider a thin material which is placed either next to a mirror (Figure 2a,b) or in the middle of the cavity (Figure 2c,d). We choose L_y = 20000 au and a thickness $l_y=\delta l_y\cdot N_y=2000\ll L_y$ with δl_y = 20 au and N_y = 100. The light–matter coupling used in Figure 2a–d is g_c = 5 meV, where $g_k=\sqrt{\frac{\omega_c(k_x,k_y)}{\omega_c(0,\pi/L_y)}}g_c$, and for the matter parameters we choose ω_0 = 2.2 eV with τ_x = 150 cm^{-1}. The position of each layer of matter is given by $Y_m=\left(m+\frac{1}{2}\right)\delta l_y$. Here, we include five energetically relevant cavity modes with $k_y\le 5\frac{\pi}{L_y}$.

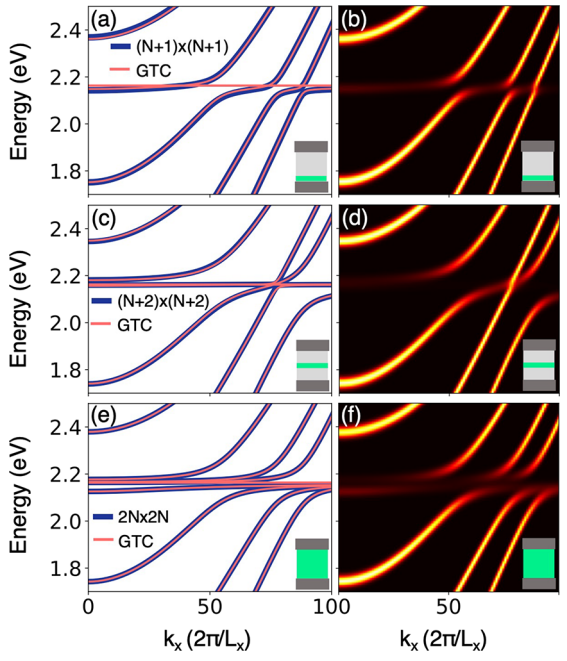

Figure 2. Polariton dispersion for thin material placed (a, b) near a cavity mirror, (c, d) placed in the middle, and a (e, f) filled cavity. (a), (c), and (e) Polariton dispersion computed from the generalized Tavis–Cummings Hamiltonian compared to the $(N+1)\times(N+1)$ model in (a), $(N+2)\times(N+2)$ model in (c), and $2N\times 2N$ model in (e). Corresponding absorption spectra for the coupled molecule–cavity hybrid system in (b), (d), and (f).

Figure 2a shows that the $(N+1)\times(N+1)$ model shown in Figure 1g (see eq S24 in the SI) provides visually identical results compared to direct diagonalization of $\mathcal{H}_{GTC}(k_z=0)$ given in eq 1. Note that direct diagonalization also shows the dark matter states which we ignore while constructing the $(N+1)\times(N+1)$ model. These dark states do not show up in the absorption (visibility) spectrum as they do not have any photonic contributions. This can be observed in Figure 2b, which presents the absorption spectrum[24,40] of the coupled cavity–matter system given by

$$I_A(\omega,k_x)=\sum_i|\langle P_{i,k_x}|\sum_{k_y}\hat{a}_{k_x,k_y}^{\dagger}|G,0\rangle|^2 e^{-(\mathcal{E}_{i,k_x}-E_G-\omega)^2/2\Gamma_c^2} \tag{7}$$

where $|P_{i,k_x}\rangle$is the ith polaritonic state that is an eigenstate of $\hat{h}_{GTC}(k_x)$ with energy $\mathcal{E}_{i,k_x}$, and E_G is the energy of $|G,0\rangle$. Here Γ_c = 15 meV accounts for various sources of dissipation phenomenologically, such as cavity loss.

In Figure 2c,d we consider a material placed in the middle of the cavity such that $Y_m=\frac{L_y}{2}-\frac{l_y}{2}+m\cdot\delta l_y$. Figure 2c shows that the $(N+2)\times(N+2)$ model shown in Figure 1f (see eqs S30 and S31 in the SI) correctly predicts the polariton bands in comparison to the numerical results obtained by directly diagonalizing $\hat{h}_{GTC}(k_x)$. Note that in Figure 2a,b the anticrossings grow gradually larger with respect to the k_y of the cavity mode (which scales as $k_y^{3/2}$ as shown in the SI). By contrast, Figure 2c,d shows that the anticrossings are large for odd k_y while they are negligible for even k_y, as the spatial dependence for even cavity modes becomes zero at the center of the cavity.

Figure 2e,f presents the dispersion and absorption spectra for a filled cavity. Here, we use g_c = 2 meV and use N_y = 999 with $Y_0=\frac{\delta l_y}{2}=10$ and the rest of the parameters are maintained as in Figure 2a–d. Figure 2e presents the corresponding multimode polariton dispersion computed numerically by diagonalizing eq 1 compared with the $2N\times 2N$ model in eq S19 in the SI. The $2N\times 2N$ model reproduces the band dispersion, as expected. Overall, the results in Figure 2 demonstrate the validity of the approximate semianalytical models.

In Figure 3 we explore how the spatial location and the thickness of the material modify the polariton dispersion. In Figure 3a-c we present the polariton bands as a function of N_y (number of layers) at various k_x values while keeping g_c = 4.743 meV a constant. Our numerical results show that the polariton dispersion at N_y = 1 (single layer) and N_y = 999 (filled) can be obtained using the $(N+1)\times(N+1)$ and the $2N\times 2N$ models, respectively. For any intermediate values of N_y, i.e. partially filled cavities, an accurate polariton dispersion can be obtained using the general $(N+N_e)\times(N+N_e)$ model given in eq 6. Similarly, Figure 3d–f presents the polariton bands at three specific values of k_x and as a function of the material location Y_0. Here we use g_c = 4.743 meV while the rest of the parameters are the same as in Figure 2a. The numerical results show that the in the limiting scenarios, at $Y_0=\frac{\delta l_y}{2}=10$ au and $Y_0=\frac{L_y-l_y}{2}=9000$ au, the polariton dispersion can be

https://doi.org/10.1021/acs.nanolett.3c01017
Nano Lett. 2023, 23, 4082–4089

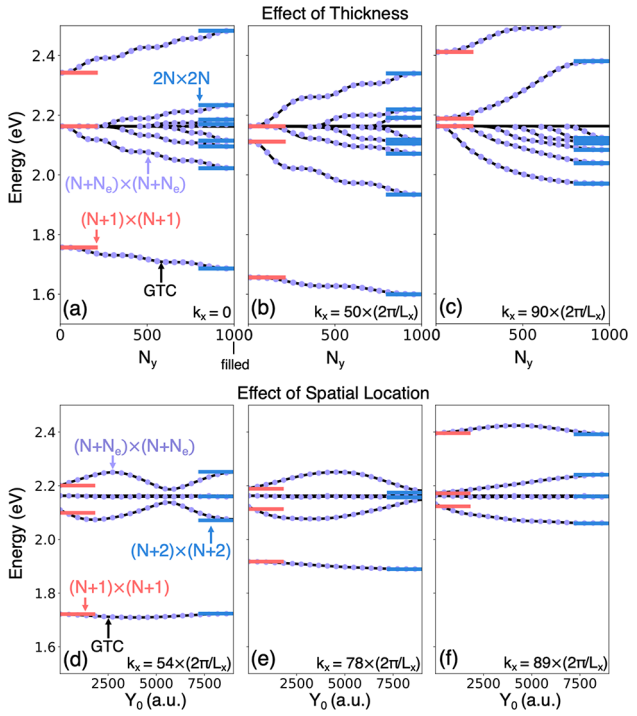

Figure 3. (a–c) Polariton dispersion as a function of the number of layers N_y at various k_x computed from the generalized Tavis–Cummings (GTC) Hamiltonian compared to the predictions of the generalized $2N \times 2N$ (at $N_y = 999$) model and the $(N + 1) \times (N + 1)$ (at $N_y = 1$). (d–f) Polariton dispersion as a function of the position of the material inside the cavity (Y_0 is the position of the first layer of the material) at various k_x computed from the generalized Tavis–Cummings (GTC) Hamiltonian compared to the predictions of $(N + 1) \times (N + 1)$ and $(N + 2) \times (N + 2)$ models.

obtained by the $(N + 2) \times (N + 2)$ and $(N + 1) \times (N + 1)$ models, respectively.

Overall, we numerically demonstrate that the general $(N + N_e) \times (N + N_e)$ model can be used to compute the multimode polariton dispersion for arbitrary geometries of multilayered materials. We demonstrated that in specific scenarios, simplified models such as $2N \times 2N$, $(N + 1) \times (N + 1)$, and $(N + 2) \times (N + 2)$ can be used to compute the polariton dispersion. Our work sheds light on the recently discussed ambiguity[21,22,26,41−43] of using $(N + 1) \times (N + 1)$ and $2N \times 2N$ models for fitting experimental dispersion. While for single-layer thin materials the $(N + 1) \times (N + 1)$ model is appropriate, the $2N \times 2N$ model is appropriate for obtaining polariton dispersions in filled cavities. However, our results suggest that the general $(N + N_e) \times (N + N_e)$ model should be used in all circumstances for extracting parameters related to light–matter coupling.

Comparison with Experiment. Here we implement the general $(N + N_e) \times (N + N_e)$ model to compute the multimode polariton dispersion for a multilayered perovskite material and compare to the experimentally obtained reflectance spectrum. We prepare the multilayered 2D perovskite material $BA_2(MA)_2Pb_3I_{10}$, where BA = $CH_3(CH_2)_3NH_3$ and MA = CH_3NH_3, that is sandwiched between Ag and Au layers that act as mirrors. We also use a poly(methyl methacrylate) (PMMA) layer as a spacer to extend the quantization length of the cavity when making partially filled cavities. Experimental details can be found in the SI. Note that the layers of the perovskite material can be considered noninteracting, thus allowing us to directly implement the general $(N + N_e) \times (N + N_e)$ model to obtain the multimode polariton dispersion.

Figure 4 presents the multimode polariton dispersion obtained experimentally via the reflectance spectra. Figure 4a shows the reflectance spectra obtained for a filled cavity. To obtain the theoretical multimode polariton dispersion, we model the matter as a dispersionless material with a matter excitation energy of $\omega_0 = 2.05$ eV (such that $\varepsilon(k_x) = \omega_0$) and a refractive index of $\eta_{PX} = 2.35$.[44] We directly use this refractive index to obtain the uncoupled photon band dispersion $\omega_c(\boldsymbol{k}) = \frac{c}{\eta}|\boldsymbol{k}|$ for the filled cavity presented in Figure 4a. We use an individual layer thickness of $\delta l_y = 50$ au[45] Note that for $\delta l_y \ll l_y$, the explicit value of the δl_y does not matter. We find $g_c \approx 3.9$ meV (such that $g_k = \sqrt{\frac{\omega_c(k_x,k_y)}{\omega_c(0,\pi/L_y)}}\, g_c$) and $L_y \approx 18122$ au through fitting and considering four cavity mode branches with $k_y \in \left\{\frac{5\pi}{L_y}, \frac{6\pi}{L_y}, \frac{7\pi}{L_y}, \frac{8\pi}{L_y}\right\}$, for constructing the general $(N + N_e) \times (N + N_e)$ matrix. In addition to this we can also construct approximate $(N + N_e) \times (N + N_e)$ models by ignoring weakly coupled excitonic branches. A numerical way to perform this approximation is by using a tolerance factor ε_{tol} (set to 0.1 here), below which the singular values are considered to be 0 when checking for linear independence when constructing Λ_{NO}. The dispersion obtained with the general $(N + N_e) \times (N + N_e)$ model (dashed lines) and the approximate $(N + N_e) \times (N + N_e)$ model (black circles) is overlaid on the experimentally obtained reflectance in Figure 4a–c, showing good agreement. Note that the upper polariton branches are not visible in the experimental dispersion here because the thick semiconductor absorbs too much above-gap light.[46,47]

In Figure 4a only the two parameters g_c and L_y are used for fitting the experimental dispersion. The numerically computed approximate $(N + N_e) \times (N + N_e)$ matrix model at $k_x = 0$ is shown in Figure 4d, which exactly takes the form of the widely used $2N \times 2N$ model.[21−23,26]

Next in Figure 4b we manufacture a partially filled cavity by using PMMA as a spacer. The refractive index of the PMMA is $\eta_{PMMA} = 1.5$. For a cavity filled with materials of different refractive indexes, we obtain an effective refractive index through fitting such that $1.5 < \eta < 2.35$. Here we obtain the length of the perovskite material $l_y = 4300$ au, the length of the cavity $L_y \approx 24143$ au, $g_c \approx 6.8$ meV, and the effective refractive index $\eta = 1.65$ by fitting the dispersion curves visually. Here we have considered six energetically relevant cavity mode branches with $k_y \in \left\{\frac{3\pi}{L_y}, \frac{4\pi}{L_y}, \frac{5\pi}{L_y}, \frac{6\pi}{L_y}, \frac{7\pi}{L_y}, \frac{8\pi}{L_y}\right\}$. These parameters fit the dispersion with reasonable accuracy. The numerically computed approximate $(N + N_e) \times (N + N_e)$ matrix at $k_x = 0$ is shown in Figure 4e for the case shown in Figure 4b. As can be seen here, the matrix has a $(N + 2) \times (N + 2)$ structure with a very complex set of couplings.

Finally, in Figure 4c we show results after fabrication of partially filled cavities with the material placed near the center of the cavity. Here, we fit and obtain $L_y = 24691$ au, $l_y = 4400$ au, $\eta = 1.63$, and $g_c \approx 5.6$ meV and additionally find the location of the material $Y_0 = 4.9 \times L_y$, by visually fitting the dispersion. Here we have considered six energetically relevant cavity mode branches (third to eighth cavity mode branches along y). The corresponding approximate $(N + N_e) \times (N +$

https://doi.org/10.1021/acs.nanolett.3c01017
Nano Lett. 2023, 23, 4082−4089

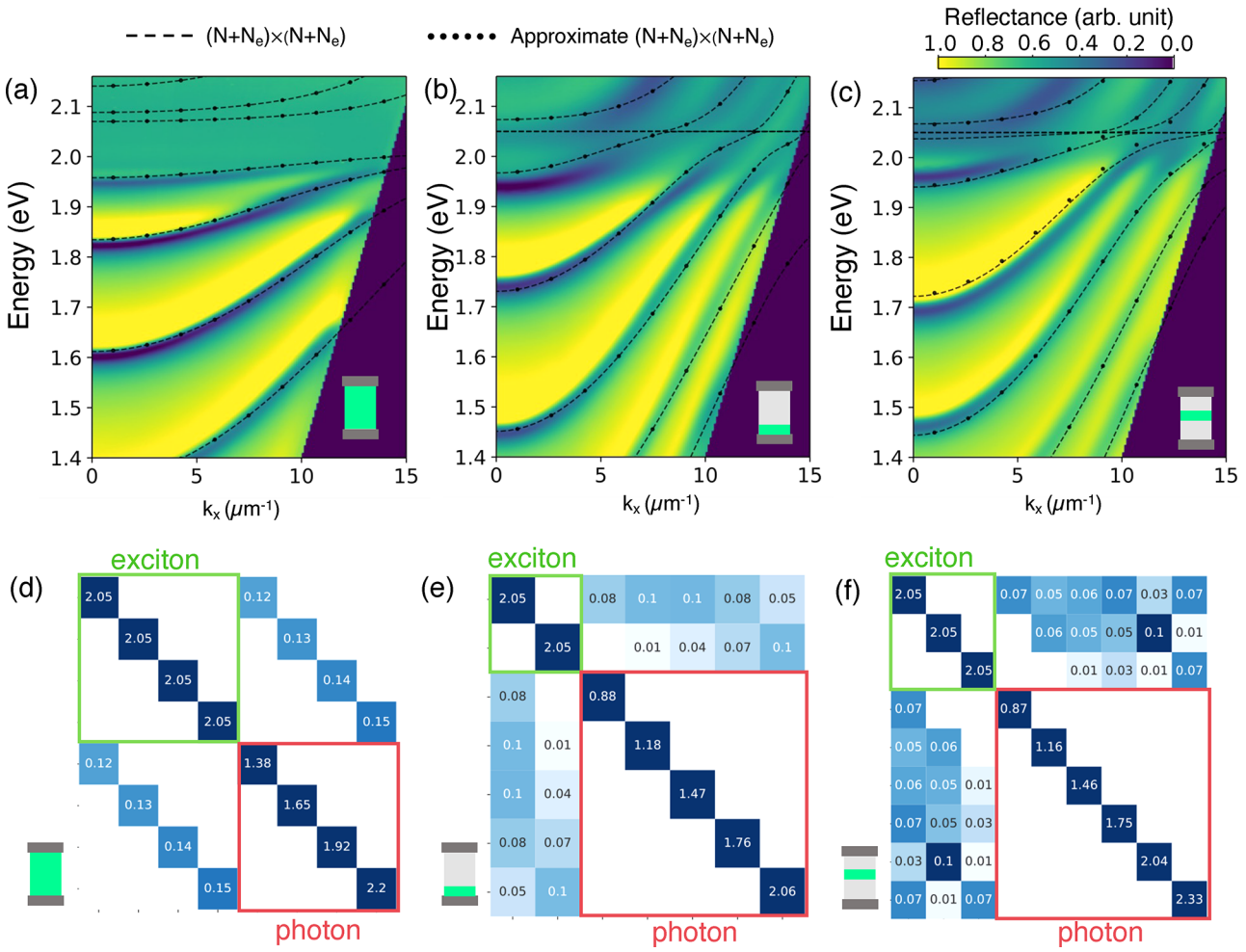

Figure 4. Experimental dispersion obtained from Fourier-plane (angle-resolved) white light reflectance microscopy for three different structures depicted in the lower-right corner of each panel. (a–c) The experimental results are compared to theoretical predictions for three different structures: (a) filled cavity, (b) material placed beside a mirror, and (c) material placed near the middle of the cavity. The experimental results are compared to theoretical predictions, where the dashed lines represent the predictions using the general $(N + N_e) \times (N + N_e)$ model and the dotted lines represent the predictions using the approximate $(N + N_e) \times (N + N_e)$ model. (d–f) The matrix structures of the approximate $(N + N_e) \times (N + N_e)$ model corresponding to (a–c) with values in eV.

N_e) matrix at $k_x = 0$ is shown in Figure 4f for the case shown in Figure 4c which has a $(N + 3) \times (N + 3)$ structure with a complex set of couplings. In all cases we capture all of the subtle features of the experimental dispersion with reasonable accuracy.

Transfer matrix simulations corresponding to each experimental configuration are shown in Figure S2, showing excellent agreement with experiments. Thus, it is likely that small discrepancies (in Figure 4b,c) between our microscopic model and experiments are due to the use of idealized cavity mode functions which may be remedied by obtaining them using the Helmholtz equation.

Here, we presented a microscopic theory for obtaining multimode polariton dispersion of a material inside a cavity. Starting with the GTC Hamiltonian, we developed a general strategy to obtain the polariton dispersion in multimode cavities, which takes the form of a general $(N + N_e) \times (N + N_e)$ model. Unlike the widely used $2N \times 2N$ or $(N + 1) \times (N + 1)$ models, our approach can be used for a material of arbitrary thickness and position within the cavity to obtain the multimode polariton dispersion. In contrast to previous approaches of directly fitting matrix elements, our method relies on structural parameters like the thickness and location of the material inside the cavity. We show that in certain scenarios, the general $(N + N_e) \times (N + N_e)$ model reduces to the widely used $2N \times 2N$ (for a filled cavity) model or the $(N + 1) \times (N + 1)$ (single or thin layer placed beside a mirror) model and find other interesting models such as the $(N + 2) \times (N + 2)$ model that describes a thin material placed in the middle of the cavity.

In this work we have employed a simple tight-binding model for matter and considered idealized cavity mode functions. Our approach can be generalized to using *ab initio* electronic structure theory and using more realistic cavity mode functions obtained from solving Maxwell's equations, which will be investigated in future work.

■ ASSOCIATED CONTENT

Supporting Information

The Supporting Information is available free of charge at https://pubs.acs.org/doi/10.1021/acs.nanolett.3c01017.

Derivation of the dipole gauge Hamiltonian and exciton–polariton Hamiltonian, transfer matrix simulation, discussion on mode-truncation, self-consistent

https://doi.org/10.1021/acs.nanolett.3c01017
Nano Lett. 2023, 23, 4082–4089

treatment of refractive index and matrix models, and experimental details (PDF)

AUTHOR INFORMATION

Corresponding Authors

Arkajit Mandal − *Department of Chemistry, Columbia University, New York, New York 10027, United States;* orcid.org/0000-0001-9088-2980; Email: am5815@columbia.edu

David R. Reichman − *Department of Chemistry, Columbia University, New York, New York 10027, United States;* Email: drr2103@columbia.edu

Authors

Ding Xu − *Department of Chemistry, Columbia University, New York, New York 10027, United States*

Ankit Mahajan − *Department of Chemistry, Columbia University, New York, New York 10027, United States*

Joonho Lee − *Department of Chemistry, Columbia University, New York, New York 10027, United States;* orcid.org/0000-0002-9667-1081

Milan Delor − *Department of Chemistry, Columbia University, New York, New York 10027, United States;* orcid.org/0000-0002-9480-9235

Complete contact information is available at: https://pubs.acs.org/10.1021/acs.nanolett.3c01017

Notes

The authors declare no competing financial interest.

ACKNOWLEDGMENTS

This work was supported by the NSF-1954791 (A.M. and D.R.R.) and NSF CHE-2203844 (M.D. and D.X.). We acknowledge the services provided by XSEDE (TG-CHE210085) and the OSG Consortium,[48,49] supported by the NSF awards #2030508 and #1836650.

REFERENCES

(1) Hutchison, J. A.; Schwartz, T.; Genet, C.; Devaux, E.; Ebbesen, T. W. Modifying Chemical Landscapes by Coupling to Vacuum Fields. *Angew. Chem., Int. Ed.* **2012**, *51*, 1592−1596.

(2) Feist, J.; Galego, J.; Garcia-Vidal, F. J. Polaritonic Chemistry with Organic Molecules. *ACS Photonics* **2018**, *5*, 205−216.

(3) Thomas, A.; Lethuillier-Karl, L.; Nagarajan, K.; Vergauwe, R. M. A.; George, J.; Chervy, T.; Shalabney, A.; Devaux, E.; Genet, C.; Moran, J.; et al. Tilting a ground-state reactivity landscape by vibrational strong coupling. *Science* **2019**, *363*, 615−619.

(4) Garcia-Vidal, F. J.; Ciuti, C.; Ebbesen, T. W. Manipulating matter by strong coupling to vacuum fields. *Science* **2021**, *373*, eabd0336.

(5) Nagarajan, K.; Thomas, A.; Ebbesen, T. W. Chemistry under Vibrational Strong Coupling. *J. Am. Chem. Soc.* **2021**, *143*, 16877−16889.

(6) Ribeiro, R. F.; Martínez-Martínez, L. A.; Du, M.; Gonzalez-Angulo, J. C.; Yuen-Zhou, J. Polariton chemistry: controlling molecular dynamics with optical cavities. *Chem. Sci.* **2018**, *9*, 6325−6339.

(7) Mandal, A.; Krauss, T. D.; Huo, P. Polariton-Mediated Electron Transfer via Cavity Quantum Electrodynamics. *J. Phys. Chem. B* **2020**, *124*, 6321−6340.

(8) Semenov, A.; Nitzan, A. Electron transfer in confined electromagnetic fields. *J. Chem. Phys.* **2019**, *150*, 174122.

(9) Wu, W.; Sifain, A. E.; Delpo, C. A.; Scholes, G. D. Polariton enhanced free charge carrier generation in donor-acceptor cavity systems by a second-hybridization mechanism. *J. Chem. Phys.* **2022**, *157*, 161102.

(10) Mandal, A.; Taylor, M.; Weight, B.; Koessler, E.; Li, X.; Huo, P. Theoretical Advances in Polariton Chemistry and Molecular Cavity Quantum Electrodynamics. 2022, 2022-g9lr7. *ChemRxiv*. https://chemrxiv.org/engage/chemrxiv/article-details/63903eee92f084c9612a9086 (accessed April 24, 2023).

(11) Li, T. E.; Cui, B.; Subotnik, J. E.; Nitzan, A. Molecular Polaritonics: Chemical Dynamics Under Strong Light-Matter Coupling. *Annu. Rev. Phys. Chem.* **2022**, *73*, 43−71.

(12) Berghuis, A. M.; Tichauer, R. H.; de Jong, L. M. A.; Sokolovskii, I.; Bai, P.; Ramezani, M.; Murai, S.; Groenhof, G.; Rivas, J. G. Controlling Exciton Propagation in Organic Crystals through Strong Coupling to Plasmonic Nanoparticle Arrays. *ACS Photonics* **2022**, *9*, 2263−2272.

(13) Xu, D.; Mandal, A.; Baxter, J. M.; Cheng, S.-W.; Lee, I.; Su, H.; Liu, S.; Reichman, D. R.; Delor, M. Ultrafast imaging of coherent polariton propagation and interactions. 2022, 2205.01176. arXiv. https://arxiv.org/abs/2205.01176 (accessed April 24, 2023).

(14) Deng, H.; Haug, H.; Yamamoto, Y. Exciton-polariton Bose−Einstein condensation. *Rev. Mod. Phys.* **2010**, *82*, 1489−1537.

(15) Frisk Kockum, A.; Miranowicz, A.; De Liberato, S.; Savasta, S.; Nori, F. Ultrastrong coupling between light and matter. *Nat. Rev. Phys.* **2019**, *1*, 19−40.

(16) Keeling, J.; Kéna-Cohen, S. Bose−Einstein Condensation of Exciton-Polaritons in Organic Microcavities. *Annu. Rev. Phys. Chem.* **2020**, *71*, 435−459.

(17) Arnardottir, K. B.; Moilanen, A. J.; Strashko, A.; Törmä, P.; Keeling, J. Multimode Organic Polariton Lasing. *Phys. Rev. Lett.* **2020**, *125*, 233603.

(18) Rozenman, G. G.; Akulov, K.; Golombek, A.; Schwartz, T. Long-Range Transport of Organic Exciton-Polaritons Revealed by Ultrafast Microscopy. *ACS Photonics* **2018**, *5*, 105−110.

(19) Perez-Sanchez, J. B.; Yuen-Zhou, J. Polariton Assisted Down-Conversion of Photons via Nonadiabatic Molecular Dynamics: A Molecular Dynamical Casimir Effect. *J. Phys. Chem. Lett.* **2020**, *11*, 152−159.

(20) Mandal, A.; Vega, S. M.; Huo, P. Polarized Fock States and the Dynamical Casimir Effect in Molecular Cavity Quantum Electrodynamics. *J. Phys. Chem. Lett.* **2020**, *11*, 9215−9223.

(21) Georgiou, K.; McGhee, K. E.; Jayaprakash, R.; Lidzey, D. G. Observation of photon-mode decoupling in a strongly coupled multimode microcavity. *J. Chem. Phys.* **2021**, *154*, 124309.

(22) Richter, S.; Michalsky, T.; Fricke, L.; Sturm, C.; Franke, H.; Grundmann, M.; Schmidt-Grund, R. Maxwell consideration of polaritonic quasi-particle Hamiltonians in multi-level systems. *Appl. Phys. Lett.* **2015**, *107*, 231104.

(23) Michetti, P.; La Rocca, G. Polariton states in disordered organic microcavities. *Phys. Rev. B* **2005**, *71*, 115320.

(24) Tichauer, R. H.; Feist, J.; Groenhof, G. Multi-scale dynamics simulations of molecular polaritons: The effect of multiple cavity modes on polariton relaxation. *J. Chem. Phys.* **2021**, *154*, 104112.

(25) Gerace, D.; Andreani, L. C. Quantum theory of exciton-photon coupling in photonic crystal slabs with embedded quantum wells. *Phys. Rev. B* **2007**, *75*, 235325.

(26) Balasubrahmaniyam, M.; Genet, C.; Schwartz, T. Coupling and decoupling of polaritonic states in multimode cavities. *Phys. Rev. B* **2021**, *103*, L241407.

(27) Keeling, J. *Light-Matter Interactions and Quantum Optics*; University of St. Andrews: 2012.

(28) Li, J.; Golez, D.; Mazza, G.; Millis, A. J.; Georges, A.; Eckstein, M. Electromagnetic coupling in tight-binding models for strongly correlated light and matter. *Phys. Rev. B* **2020**, *101*, 205140.

(29) Dmytruk, O.; Schiró, M. Gauge fixing for strongly correlated electrons coupled to quantum light. *Phys. Rev. B* **2021**, *103*, 075131.

(30) Medina, I.; García-Vidal, F. J.; Fernández-Domínguez, A. I.; Feist, J. Few-Mode Field Quantization of Arbitrary Electromagnetic Spectral Densities. *Phys. Rev. Lett.* **2021**, *126*, 093601.

(31) Feist, J.; Fernández-Domínguez, A. I.; García-Vidal, F. J. Macroscopic QED for quantum nanophotonics: emitter-centered modes as a minimal basis for multiemitter problems. *Nanophotonics* **2020**, *10*, 477−489.
(32) Schäfer, C.; Johansson, G. Shortcut to Self-Consistent Light-Matter Interaction and Realistic Spectra from First Principles. *Phys. Rev. Lett.* **2022**, *128*, 156402.
(33) Passler, N. C.; Jeannin, M.; Paarmann, A. Layer-resolved absorption of light in arbitrarily anisotropic heterostructures. *Phys. Rev. B* **2020**, *101*, 165425.
(34) Mattheakis, M.; Valagiannopoulos, C. A.; Kaxiras, E. Epsilon-near-zero behavior from plasmonic Dirac point: Theory and realization using two-dimensional materials. *Phys. Rev. B* **2016**, *94*, 201404.
(35) Graf, A.; Tropf, L.; Zakharko, Y.; Zaumseil, J.; Gather, M. C. Near-infrared exciton-polaritons in strongly coupled single-walled carbon nanotube microcavities. *Nat. Commun.* **2016**, *7*, 13078.
(36) Dietrich, C. P.; Steude, A.; Tropf, L.; Schubert, M.; Kronenberg, N. M.; Ostermann, K.; Höfling, S.; Gather, M. C. An exciton-polariton laser based on biologically produced fluorescent protein. *Science advances* **2016**, *2*, e1600666.
(37) Coles, D. M.; Lidzey, D. G. A ladder of polariton branches formed by coupling an organic semiconductor exciton to a series of closely spaced cavity-photon modes. *Appl. Phys. Lett.* **2014**, *104*, 191108.
(38) Orosz, L.; Reveret, F.; Bouchoule, S.; Zúñiga-Pérez, J.; Médard, F.; Leymarie, J.; Disseix, P.; Mihailovic, M.; Frayssinet, E.; Semond, F.; et al. Fabrication and optical properties of a fully-hybrid epitaxial ZnO-based microcavity in the strong-coupling regime. *Applied physics express* **2011**, *4*, 072001.
(39) Faure, S.; Brimont, C.; Guillet, T.; Bretagnon, T.; Gil, B.; Médard, F.; Lagarde, D.; Disseix, P.; Leymarie, J.; Zúñiga-Pérez, J.; et al. Relaxation and emission of Bragg-mode and cavity-mode polaritons in a ZnO microcavity at room temperature. *Appl. Phys. Lett.* **2009**, *95*, 121102.
(40) Lidzey, D. G.; Bradley, D. D. C.; Armitage, A.; Walker, S.; Skolnick, M. S. Photon-Mediated Hybridization of Frenkel Excitons in Organic Semiconductor Microcavities. *Science* **2000**, *288*, 1620−1623.
(41) Georgiou, K.; Jayaprakash, R.; Othonos, A.; Lidzey, D. G. Ultralong-Range Polariton-Assisted Energy Transfer in Organic Microcavities. *Angew. Chem.* **2021**, *133*, 16797−16803.
(42) Menghrajani, K. S.; Barnes, W. L. Strong Coupling beyond the Light-Line. *ACS Photonics* **2020**, *7*, 2448−2459.
(43) Tagami, T.; Ueda, Y.; Imai, K.; Takahashi, S.; Mizuno, H.; Yanagi, H.; Obuchi, T.; Nakayama, M.; Yamashita, K. Anisotropic light-matter coupling and below-threshold excitation dynamics in an organic crystal microcavity. *Opt. Express* **2021**, *29*, 26433−26443.
(44) Song, B.; Hou, J.; Wang, H.; Sidhik, S.; Miao, J.; Gu, H.; Zhang, H.; Liu, S.; Fakhraai, Z.; Even, J.; et al. Determination of Dielectric Functions and Exciton Oscillator Strength of Two-Dimensional Hybrid Perovskites. *ACS Materials Letters* **2021**, *3*, 148−159.
(45) Mao, L.; Stoumpos, C. C.; Kanatzidis, M. G. Two-dimensional hybrid halide perovskites: principles and promises. *J. Am. Chem. Soc.* **2019**, *141*, 1171−1190.
(46) Fieramosca, A.; Polimeno, L.; Ardizzone, V.; Marco, L. D.; Pugliese, M.; Maiorano, V.; Giorgi, M. D.; Dominici, L.; Gigli, G.; Gerace, D.; et al. Two-dimensional hybrid perovskites sustaining strong polariton interactions at room temperature. *Science Advances* **2019**, *5*, eaav9967.
(47) Wang, J.; Su, R.; Xing, J.; Bao, D.; Diederichs, C.; Liu, S.; Liew, T. C.; Chen, Z.; Xiong, Q. Room Temperature Coherently Coupled Exciton-Polaritons in Two-Dimensional Organic-Inorganic Perovskite. *ACS Nano* **2018**, *12*, 8382−8389.
(48) Sfiligoi, I.; Bradley, D. C.; Holzman, B.; Mhashilkar, P.; Padhi, S.; Wurthwein, F. The pilot way to grid resources using glideinWMS. *2009 WRI World Congress on Computer Science and Information Engineering*, 2009; pp 428−432
(49) Pordes, R.; Petravick, D.; Kramer, B.; Olson, D.; Livny, M.; Roy, A.; Avery, P.; Blackburn, K.; Wenaus, T.; Würthwein, F.; et al. The open science grid. *J. Phys. Conf. Ser.* **2007**, *78*, 012057.

https://doi.org/10.1021/acs.nanolett.3c01017
Nano Lett. 2023, 23, 4082−4089